communications earth & environment

Article

https://doi.org/10.1038/s43247-024-01493-6

CO_2 rock physics modeling for reliable monitoring of geologic carbon storage

Neala Creasy[1] ✉, Lianjie Huang[1] ✉, Erika Gasperikova[2], William Harbert[3,4], Tom Bratton[5] & Quanlin Zhou[2]

Monitoring, verification, and accounting (MVA) are crucial to ensure safe and long-term geologic carbon storage. Seismic monitoring is a key MVA technique that utilizes seismic data to infer elastic properties of CO_2-saturated rocks. Reliable accounting of CO_2 in subsurface storage reservoirs and potential leakage zones requires an accurate rock physics model. However, the widely used CO_2 rock physics model based on the conventional Biot-Gassmann equation can substantially underestimate the influence of CO_2 saturation on seismic waves, leading to inaccurate accounting. We develop an accurate CO_2 rock physics model by accounting for both effects of the stress dependence of seismic velocities in porous rocks and CO_2 weakening on the rock framework. We validate our CO_2 rock physics model using the Kimberlina-1.2 model (a previously proposed geologic carbon storage site in California) and create time-lapse elastic property models with our new rock physics method. We compare the results with those obtained using the conventional Biot-Gassmann equation. Our innovative approach produces larger changes in elastic properties than the Biot-Gassmann results. Using our CO_2 rock physics model can replicate shear-wave speed reductions observed in the laboratory. Our rock physics model enhances the accuracy of time-lapse elastic-wave modeling and enables reliable CO_2 accounting using seismic monitoring.

Carbon capture and storage (CCS) are key components in achieving the goal to significantly reduce anthropogenic emissions of greenhouse gases. Safe deployment of large-scale CCS requires monitoring, verification, and accounting (MVA) tools to assure that injectivity and capacity predictions are reliable, fate and configuration of the carbon dioxide (CO_2) plume is acceptable, regulatory permitting and for compliance, public assurance, risk reduction, and stakeholder assurance[1]. In particular, accurate accounting of subsurface CO_2 requires an understanding of how to determine the elastic properties, which control seismic wave velocities, of rocks and the corresponding changes because of CO_2 injection and migration.

Time-lapse seismic monitoring methods (e.g., surface seismic surveys, vertical seismic profiling, and cross-well seismic monitoring) provide indirect measurements of CO_2 and reservoir properties in the deep subsurface of geologic carbon storage (GCS) sites[2–4]. Rock physics models are crucial for interpreting seismic monitoring data to enable accounting of subsurface changes associated with CO_2 injection and migration, as 4D (the 3D space and time) anomalies using seismic data are converted to CO_2 saturation maps. These CO_2 saturation maps based on seismic observations are used to update CO_2 fluid migration pathways, which are necessary to assess the movement of CO_2 within the storage reservoir, plume formation/migration, and detecting leaks.

Traditionally, observed seismic anomalies are completely attributed to CO_2 saturation distribution with sustained phases of CO_2 injection over long-time periods (on the scale of tens to hundreds of years). However, seismic interpretation requires considerations into other phenomena that may change the seismic response[5]. Typically, calculating seismic velocity variations required for forward seismic modeling are calculated as a function of CO_2 saturation using the Gassmann equations[6]. The Gassmann-Biot fluid substitution theory[6,7] has been commonly employed in estimating changes in the seismic response caused by fluid injection or leakage[4,8,9] and is widely used in seismic reflection data analyses in hydrocarbon exploration and CO_2 enhanced oil recovery[10]. Since fluids have no shear modulus, the predicted changes in the S-wave velocity is very minimal (on the order of 1% change) because there is only a change in the density of the fluid phase with the injected CO_2. P-wave velocities are expected to change by 5–15% with CO_2 injection because the bulk modulus of the fluid phase changes significantly because of injected CO_2[11–13].

[1]Earth and Environmental Sciences Division, Los Alamos National Laboratory, Los Alamos, NM, USA. [2]Energy Geoscience Division, Lawrence Berkeley National Laboratory, Berkeley, CA, USA. [3]National Energy Technology Laboratory, ORISE, Pittsburgh, PA, USA. [4]University of Pittsburgh, Department of Geology and Environmental Science, Pittsburgh, PA, USA. [5]Tom Bratton, LLC, Littleton, CO, USA. ✉e-mail: nmcreasy@lanl.gov; ljh@lanl.gov

Previous studies show that sandstone that is exposed to free-phase CO_2 and brine for several months can demonstrate large changes in seismic velocities (~ 15% decrease for P-wave velocity [V_P] and ~ 16% decrease for S-wave velocity [V_S]) caused by chemical reactions between the rock and CO_2 (see more in Supplementary Note 1)[14,15]. In other experimental studies, seismic wave speeds can change negligibly or even more so that discussed here; however, these studies vary widely with the experimental setup (e.g., state of injected CO_2, the residence time, porosity, temperature, mineralogy, etc[16]). Recent geophysical observations of GCS have illustrated that the S-wave velocity can also change as much as the P-wave velocity during CO_2 injection and migration because of possible mineral dissolution[17–19]. However, estimating effects of CO_2 saturation with the Biot-Gassmann equation cannot replicate these large changes in seismic velocities because this approach only considers the impact of supercritical CO_2 on the fluid properties and does not consider the justifiably proven evidence that rocks under these conditions are stress-dependent. More specifically in this study, we refer to stress as effective/differential pressure, which is compressive pressure minus pressure within the pore space. When referring to stress, we do not mean the entire stress tensor but rather the average of the trace of the stress tensor (pressure). As a result of long-term exposure to CO_2, the reservoir storage porosity, permeability, mineralogy, and the fluid within the pores are affected by these chemical reactions resulting in changes in the overall elastic moduli (e.g., shear and bulk moduli) of the saturated rock. A misrepresentation of seismic-wave velocities would cause an inaccurate accounting for subsurface CO_2 storage, where changes in seismic-wave velocities could be inaccurately ascribed solely to CO_2 saturation.

Theoretical approaches and experiments have demonstrated that rocks are stress-dependent and behave like nonlinear elastic bodies[20]. A series of studies[21–24] demonstrated that the elastic non-linearity of rocks is related to compliant porosity (caused by grain contacts or very thin cracks, etc.), which is often a small part of the total porosity that consists of stiff (spherical, stiff) and compliant pores. As an important note, the formation of small, subcritical cracks or dissolution along grain contacts as a result of exposure to CO_2 do have different processes depending on the mineralogy, fluid interactions, porosity, grain size, etc.[16]. The stress-dependence of the compliant porosity was derived from the theory of poroelasticity under empirically-based assumptions. Closing compliant porosity with increasing differential stress explains the experimentally observed stress dependencies of seismic velocities (exponential relationship).

We develop a new CO_2 rock physics model to account for the stress-dependent relationship and the rock frame weakening effect because of chemical reactions with CO_2. We address many considerations needed for accurate CO_2 accounting in GCS[25]. Our new rock physics model takes into account changes in seismically important variables in relation to rock properties (i.e., changes in elastic properties, porosity because of chemical reactions and pressure changes), and fluid properties (i.e., fluid saturation) during CO_2 injection and migration[25]. We validate our new CO_2 rock physics model using CO_2 reservoir simulation results of the Kimberlina-1.2 model (see Section 2.2[26,27] for more details). Our new CO_2 rock physics model enables reliable accounting of CO_2 in GCS sites.

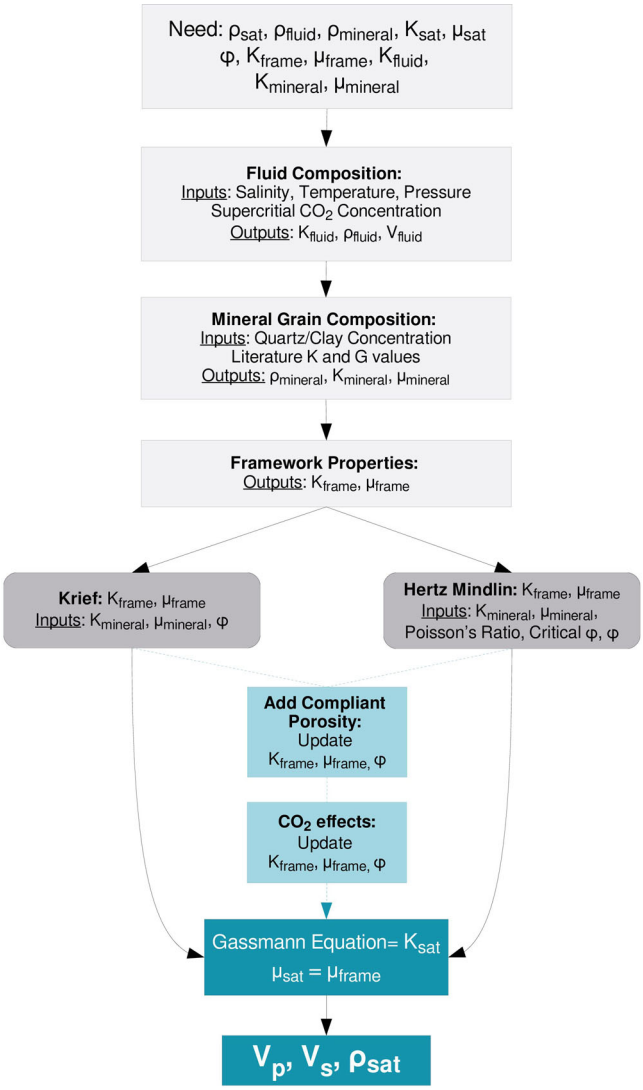

Fig. 1 | Workflow of CO_2 rock physics modeling. Workflow for calculating seismic velocities (V_P, V_S) and density (ρ_{sat}) of the saturated rock. Black arrows and gray boxes represent methods typically incorporated into rock physics modeling of GCS. Blue boxes and arrows represent the additions to this workflow explored in this paper. The first step is to calculate the fluid composition, which finds the bulk modulus (K), density (ρ), and velocity (V) of the fluid. Next is the mineral grain composition, which finds the bulk modulus (K), density(ρ), and shear modulus (μ) of the mineral grains. Third is the framework properties, such as Krief or Hertz Mindlin approaches, which calculate the framework properties. The following step is to include our proposed workflow by adding compliant porosity and CO_2 effects. Lastly, the Gassmann equation is applied to find the seismic wave speeds and density.

Stress dependence of Seismic-wave velocities because of compliant porosity

To construct a stress-dependent rock physics model, we consider compliant porosity in the construction of the bulk and shear moduli of the rock framework to account for changes in differential pressure. To calculate the resulting V_P and V_S (Fig. 1), we first calculate the bulk modulus of the fluid using published equations of state for brine and CO_2[28,29]. More details can be found in the Methods section.

The rock framework properties (K_{frame} and μ_{frame}) can be determined with various methods, but we show two possible options: Hertz-Mindlin contact theory[30] and Krief modeling[31]. The Hertz-Mindlin contact theory considers the effects of pore pressure changes in Eqs. (3) and (4) in the general case. The construction of K_{frame} with Krief modeling is empirically derived[31] based on the relationship between the properties of the rocks' composite grains and the rock frame (through the Biot poroelastic coefficient[32,33]). Therefore, if sonic log data are available, this approach is ideal in determining rock framework properties. Either approach can be used to calculate rock framework properties.

To incorporate compliant porosity, we update the bulk and shear frame moduli for compliant porosity[22] and eqs. (13) and (14). Compliant porosity data require experimental data either from the site or similar rock types. The various parameters in Eqs. (13) and (14) are important to take into account how stiff porosity (θ_s) and compliant porosity (θ_c) parameters affect the bulk modulus as a function of stress. As a result, we can use these parameters to also model porosity and incorporate compliant pores, Eq. (24). We resolve these important porosity parameters using the empirical relationship between stress and seismic-wave velocities, as described by Eqs. (18) and (19)[22,34]. Each coefficient helps to determine the various relevant parameters

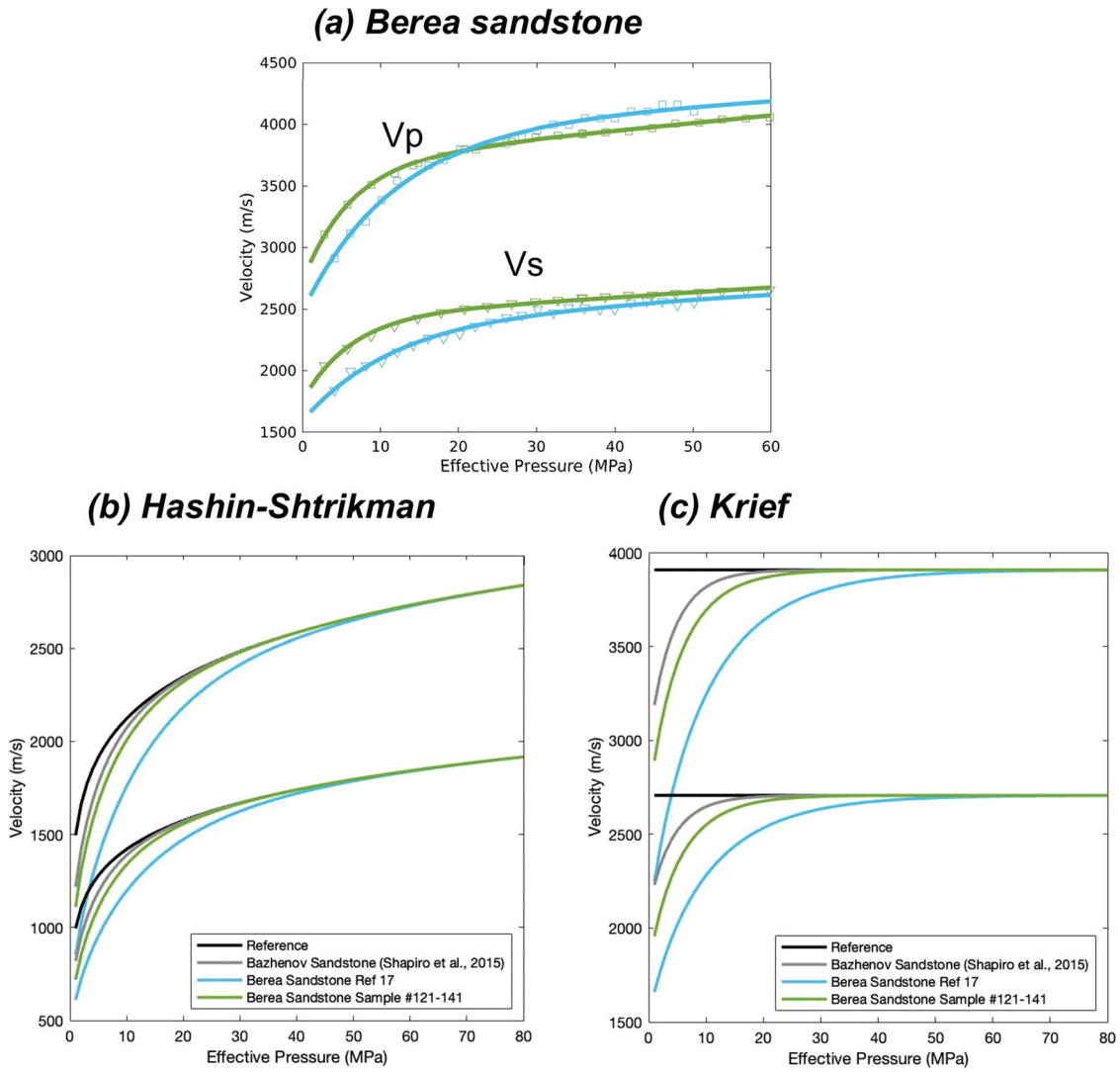

Fig. 2 | Effects of compliant porosity on seismic velocities. a Dry Berea sandstone measurements[45] for two different experiments (green squares and blue triangles). Lines represent linear least-square fits to the data with eqs. (18) and (19). **b** Estimated velocities (top set of lines = Vp and bottom set of lines = Vs) using the Hashin-Strikman from Eq. (7) and using the **c** Krief modeling from Eq. (9) by applying the compliant porosity parameters from the top image. Black lines are the reference for the methods without including compliant porosity. The gray lines are results obtained using compliant porosity parameters from[24]. All compliant porosity parameters are included in Table S1 in the supplementary information. Assumed parameters: Poisson's ratio = 0.2, $\mu_{mineral}$ = 44 GPa, $K_{mineral}$ = 33 GPa, ϕ_c = 0.4, K_{fluid} = 2.5 GPa, ϕ = 0.2.

and update the bulk and shear frame moduli using Eqs. (20) to (26). Any velocity data as a function of stress can be used for site specific lithology. Figure 2 illustrates the linear least-squares fit to two drained Berea rock samples[35]. Table S1 in the supplementary information provides the resolved coefficients. Figure 2b demonstrates the changes on theoretically-derived seismic-wave velocities using the original approach versus updating the velocities with the compliant porosity parameters from the Berea sandstone. As a result, lower effective pressures have major effects on seismic-wave velocities, where more accurate modeling agrees well with experimental studies on sandstones.

Results: rock frame changes caused by exposure to CO_2 and mineral dissolution

Previous experiments show that rock frame weakening or strengthening can occur[14,36], caused by swelling clays, dissolution of feldspars, chlorite, and carbonates[37]. One implication of rock frame alterations is an increase in microseismicity caused by increasing formation permeability and elevated pore pressure. Changes in porosity, mineral composition, or permeability result in changes in seismic-wave velocities that impact accounting of subsurface CO_2. However, it can be challenging to predict changes in seismic-wave velocities as there are complicated chemical reactions that depend on temperature, pressure, mineralogy, and brine composition. Rock samples also undergo a porosity decrease (rock strengthening) or increase (rock weakening) because of these chemical reactions[14].

We simulate a scenario under which rock frame weakening could influence seismic-wave velocities, which is associated with an increase in porosity and permeability. We use V_P and V_S ultrasonic measurements[14] on a Mt. Simon sandstone sample that underwent rock frame weakening (Fig. 3). The study measured ultrasonic V_P and V_S over a range of effective pressures (0-40 MPa) at 50 °C in a drained Mt. Simon sandstone that was pre- and post-exposed to supercritical CO_2 and brine for four weeks, resulting in V_P reduction by ~ 14%, V_S reduction by ~ 15%, and porosity increase by 8%. Since the seismic velocities of pre-exposure samples were not measured over a large range of effective pressures, we use our compliant porosity parameters from the previous section for the two Berea sandstones as reasonable compliant porosity parameters (as shown in Fig. 3), but we adjust the A_P and A_S (Eqs. (18) and (19)) parameters to fit the Mt. Simon experimental data. In Table S1 in the Supplementary Information, we use

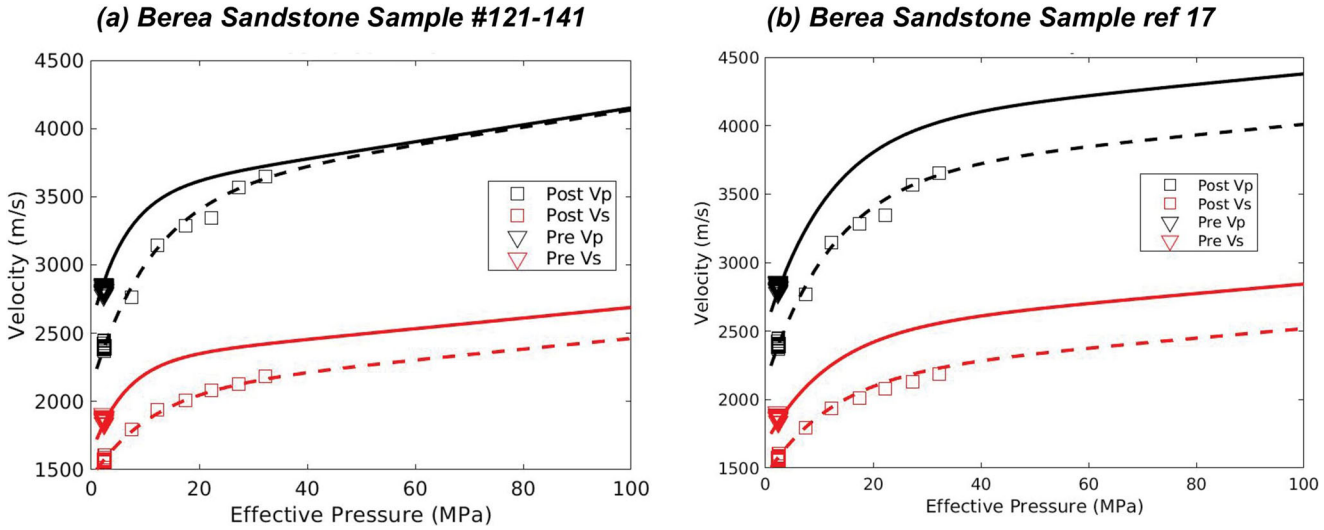

Fig. 3 | Effects of CO_2 weakening on seismic velocities. Two different models of CO_2 weakening: **a** using green-labeled Berea sandstone data (Sample #121-141) and **b** using blue-labeled Berea data (Ref. 17). We fit pre-exposure (triangles) and post-exposure (squares) to CO_2 samples[14]. Since there are limited data for pre-exposure samples, we use the two different Berea sandstone fitted parameters (see fitted parameters in Table S1) from Fig. 2.

the Kp, Ks, Bp, Bs, and D parameters from the Berea sandstones to fit the pre-exposure sample data (triangles in Fig. 3). This approach is not needed when more data are available at higher pressures, where just a standard fitting approach can be used. We employ the same fitting approach in Eqs. (18) and (19) to the post-exposure samples (Fig. 3) to accommodate changes in compliant porosity and those effects on seismic velocities.

Ideally, additional pre-exposed measurements should be made in Fig. 3 over a larger range of effective pressures; therefore, the exact changes in compliant porosity may not be accurate from the pre- to post-exposure samples. If there is dissolution of minerals, then the contribution of compliant porosity would likely increase, but it is more challenging to estimate how derivative parameters would change, such as θ_c ($K_{drys}\frac{\partial\frac{1}{K_{frame}}}{\partial\phi_c}$). Parameters θ_s and $\theta_{s\mu}$ are related to stiff porosity; these values could change somewhat between pre- and post-exposure samples because they are mainly dependent on the mineral grain bulk and shear moduli[21]. If the bulk modulus of the mineral grains decrease after CO_2 exposure (possibly caused by chemical interactions), then θ_s would decrease. This value controls the slope of the Vp curve (Fig. 3) when stiff porosity is dominated at higher effective pressures. As a result, Vp wave speeds would be lower at higher effective pressures. θ_c (how the bulk modulus changes with compliant porosity) is also dependent on the bulk and shear moduli of the mineral and the inverse of the aspect ratio of the pores. As the aspect ratio decreases, this derivative would increase. Therefore, it is challenging to predict how the aspect ratio of pore space changes as a result of CO_2 exposure without lab measurements. In general, if the aspect ratio decreases, Vp and Vs would decrease at smaller effective pressures compared with the pre-exposure samples (see Eq. (15)).

For each model point with supercritical CO_2 in the Kimberlina-1.2 model, we update the elastic moduli and porosity for long-term exposure to CO_2 and use the new fitted compliant porosity parameters from Fig. 3. All main parameters in Eqs. (18) and (19) decrease between the pre- and post-exposure sample, where compliant porosity ϕ_{c0} increases, which aligns with the observation showing porosity increase (see Table S1 in the Supplementary Information). To update the modeling for rock frame weakening, we recalculate the increase in porosity in Eq. (16) and calculate the new compliant porosity parameters and K_{drys}/μ_{drys} values in Eqs. (13) and (14). Modifying the K_{drys}/μ_{drys} values is not trivial because we have limited information on how the moduli of the minerals has changed; therefore, we simply apply a similar reduction in the elastic moduli (K_{drys}/μ_{drys}) as if the sandstones in our Kimberlina-1.2 model underwent rock frame changes similar to the Mt. Simon sandstones. We employ empirical changes in seismic velocities and porosity as a result of rock frame weakening but do not model the actual changes in mineralogy as a result of these chemical reaction. This method demonstrates how to consider the non-linearity of seismic velocity changes as a function of effective pressure. As a result, there are two mechanisms for porosity to change: non-reactive, where Eq. (14) describes how porosity is updated with the effective pressure, which is a result of the pore pressure changes; and, reactive, which occurs when there is mineral dissolution because of chemical reactions. These porosity changes then propagate throughout the model, changing the seismic velocities even more.

Discussion: accuracy of CO_2 accounting with seismic data

Dry rock frame changes because of compliant porosity or weakening/strengthening impact interpretation of time-lapse seismic monitoring of GCS and accounting of subsurface storage of CO_2. Table 1 demonstrates all the changes on different properties and how they changes as a result of compliant porosity and CO_2 weakening. Additionally, Figs. S2 and S3 in the Supporting Information show the quantitative changes of bulk and shear moduli and porosity as a function of time over the timescale of the model. Figure 4 illustrates a demonstration of CO_2 weakening on seismic-wave velocities using GCS time-lapse Kimberlina-1.2 flow simulations (see Supplementary Note 4 for more details).

We assume the entire model is sandstone for simpler modeling since CO_2 is only injected into sandstone, but shale layers are also included in the Kimberlina-1.2 model (see Supporting Note 3). We calculate seismic velocities and density of the saturated rock matrix (workflow in Fig. 1) using the compliant porosity parameters of the Berea sandstone model from Fig. 2 and the CO_2 weakening introduced in Fig. 3.

As predicted, because of CO_2 fluid substitution only, only V_p changes are significant, whereas V_S does not significantly change. However, we find that rock frame weakening and compliant porosity can also change V_P. Significant V_S changes are mainly caused by the CO_2 weakening effect as compliant porosity has only a small effect on V_S. Compliant porosity increases the porosity, which mostly influences saturated density because the pore space increases, leading to a reduction in the rock's saturated density because of the stronger influence of brine and/or supercritical CO_2.

Shear waves should be used in monitoring of geologic carbon storage because V_S changes significantly because of chemical reactions between CO_2 and the rock matrix. Modeling with compliant porosity (such as Eqs. (18) and (19)) provide a first order approximation in how porosity and

Table 1 | Changes of rock physical parameters caused by compliant porosity and CO_2 weakening

Method	Standard Gassmann Equation with Hertz-Mindlin Theory	Compliant Porosity (CP)	CP+CO_2 weakening
$\Delta\phi$	No change	increases as effective pressure decreases (Eq. (16)) because ϕ_c increases	increases when the reservoir is exposed to CO_2
ΔK	see Eq. (7)	see Eq. (13), increases with increasing differential pressure, but decreases with increasing compliant porosity	decreases as a result of increasing porosity because of CO_2 exposure and Eq. (13)
$\Delta\mu$	see Eq. (6)	see Eq. (14), increases with increasing differential pressure, but decreases with increasing compliant porosity	decreases as a result of increasing porosity because of CO_2 exposure and Eq. (14)
$\Delta\rho$	see Eq. (8)	see Eq. (17), slightly decreases when porosity increases as a result of increasing ϕ_c	see Eq. (17), slightly decreases when porosity increases as a result of increases ϕ_c and exposure to CO_2

Magnitude of changes to total porosity, bulk modulus (K), shear modulus (μ), and density (ρ) and the corresponding equations.

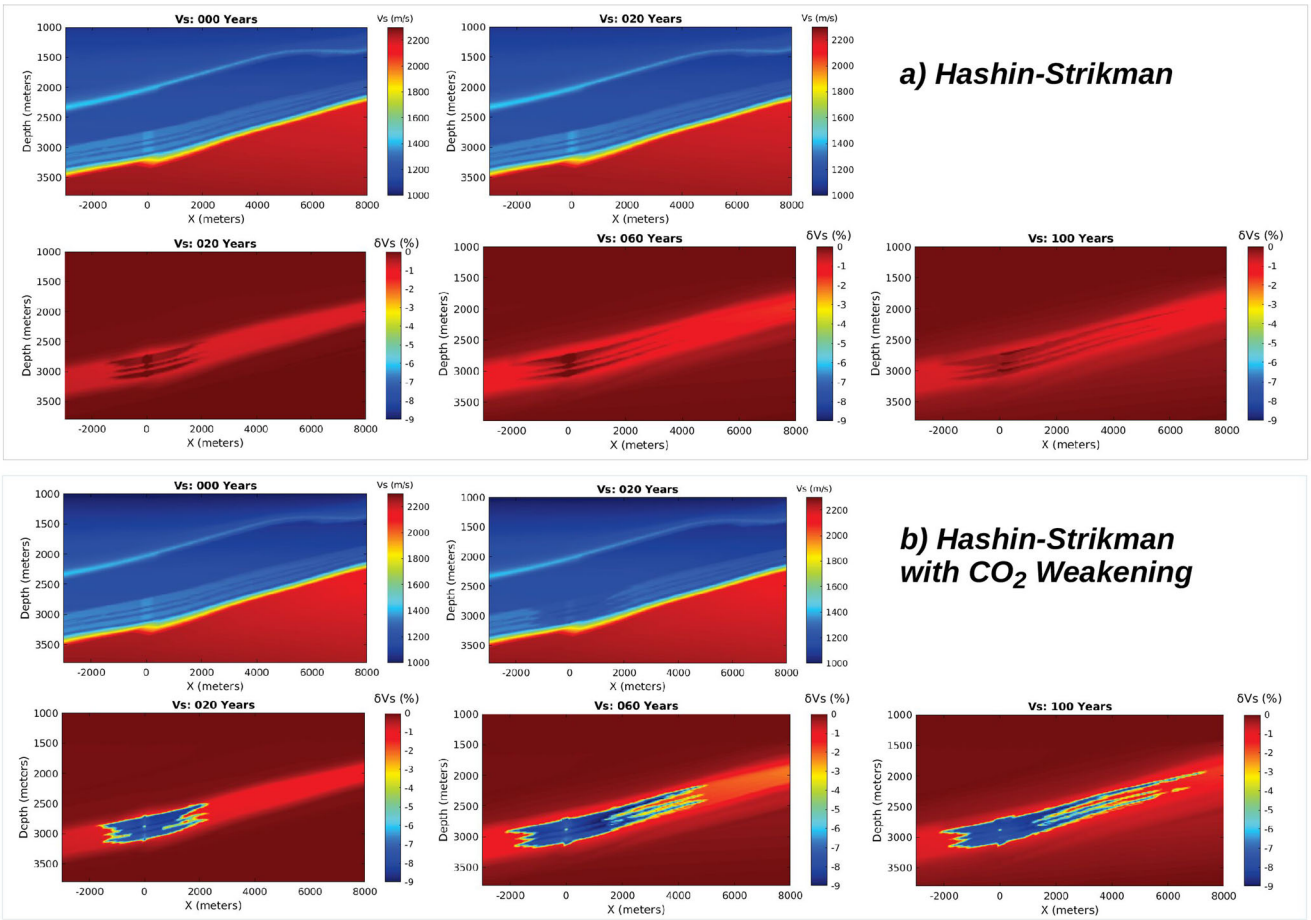

Fig. 4 | Shear-wave velocities in the Kimberlina-1.2 model. Kimberlina-1.2 model for V_s for three time steps using the **a** Hashin-Strikman approach and **b** Hashin-Strikman with the added CO_2 rock frame weakening, using the workflow in Fig. 1. The top rows illustrate two time steps (0 years and 20 years) for V_s (m/s). The bottom rows show changes in Vs relative to the baseline V_s model at 0 years in percent. The initial injection of CO_2 is at X = 0 m. The corresponding V_p and CO_2 gas saturation are described in the supplementary information.

permeability have changed because of CO_2 exposure; therefore, changes in V_P and V_S can be used for accounting of CO_2 and changes in porosity.

We provide a workflow to model changes in V_P and V_S with compliant porosity that takes into account the nonlinear relationship of seismic velocities with stress. The largest impact of this kind of modeling is that it accounts for pore pressure changes and more accurate seismic modeling of the entire reservoir, especially at lower stresses when the nonlinear relationship dominates.

More experiments are needed on chemical interactions between reservoir/cap rocks and CO_2 to constrain timing, temperature, pressure, and mineralogical conditions and the resulting changes in seismic-wave velocities and porosity. The concurrent chemical reactions are complicated and vary with a number of factors, but modeling compliant porosity opens the opportunity to include more experimental results on chemical reactions between CO_2 and the reservoir and cap rocks. If shear-wave changes exceed ~1% because of CO_2 injection, then rock framework changes have likely occurred and the resulting seismic velocity changes should not be estimated solely based on fluid substitution.

Lastly, accurate accounting of the amount of CO_2 relies on geophysical monitoring, where changes in seismic velocities cannot just be attributed to changes in gas saturation, but also changes in stress and chemical reactions between the rock framework and CO_2. However, seismic velocities provide additional information on porosity and permeability changes that improve flow imaging of CO_2 plume migration. We suggest two approaches to

improving CO_2 accounting: (1) other geophysical techniques (e.g., gravity, electromagnetic methods, etc.[38]) should be integrated with seismic velocity changes to fully account for the mass of CO_2 in the reservoir rock (these methods would be needed at high CO_2 saturations, when seismic velocity sensitivities asymptote), or (2) experiments should be performed on the different reservoir and cap rock types to evaluate the seismic velocity changes because of CO_2 injection/migration and the chemical reactions therein.

Methods

All variables defined

The following lists all variables relevant in this paper.

K_{sat} = the saturated bulk modulus
K_{frame} = the bulk modulus of the dry rock matrix
$K_{mineral}$ = the bulk modulus of the mineral grains
K_{fluid} = the bulk modulus of the fluid
K_{brine} = the bulk modulus of the brine
K_{CO_2} = the bulk modulus of supercritical CO_2
K_{drm} = the bulk modulus of the drained rock frame with compliant porosity included
ρ_{sat} = the saturated rock density
ρ_{fluid} = the density of the fluid in the pore space
ρ_{brine} = the density of the brine in the pore space
ρ_{CO_2} = the density of supercritical CO_2 in the pore space
$\rho_{mineral}$ = the density of mineral grains
ρ_{matrix} = the density of the dry rock matrix
S_g = volume fraction of gas saturation in pore space
S_w = volume fraction of brine saturation in pore space ($S_w = 1 - S_g$)
ϕ = porosity
ϕ_c = critical porosity
μ_{sat} = the shear modulus of the saturated bulk modulus
μ_{frame} = the shear modulus of the drained rock matrix
$\mu_{mineral}$ = the shear modulus of the mineral grains
μ_{drm} = the shear modulus of the drained rock frame with compliant porosity included
C = average number of contacts per spherical grain, $C = 2.8/\phi_c$
p_d = effective pressure (also known as differential pressure), $p_d = p_c - p_p$, where p_c is the confining pressure and p_p is pore pressure
ν = Poisson ratio
n = exponent derived empirically for Krief modeling, n = 3 for most sandstones
ϕ_{c0} = compliant porosity (thin, oblate cracks) in the unloaded case ($p_d = 0$)
ϕ_{s0} = stiff porosity in the unloaded case
θ_c/θ_s = how bulk modulus changes with compliant/stiff porosity, dimensionless
$\theta_{c\mu}/\theta_{s\mu}$ = how shear modulus changes with compliant/stiff porosity, dimensionless
ϕ_0 = initial porosity or assumed stiff porosity
V_{Pdry}/V_{Sdry} = seismic velocities of a dry rock matrix
V_{Pdrys}/V_{Sdrys} = seismic velocities of a dry rock matrix with compliant pores closed
K_{drys}/μ_{drys} = bulk/shear modulus of a dry rock matrix with compliant pores closed

Calculation of fluid and mineral properties

The bulk modulus and density of effective pore fluid (K_{fluid} and ρ_{fluid}) can be estimated (Eqs. [(1)] and [(2)]) using inverse bulk modulus averaging[39] and arithmetic averaging of densities of the separate fluid phases (brine phase and supercritical CO_2 phase), respectively[40]. The fluid composition requires salinity, temperature, pressure, and gas saturation to determine the bulk modulus of the fluid (K_{fluid}), density of the fluid (ρ_{fluid}), and thus the velocity of the fluid (V_{fluid}). Within this formation of calculating sound speed of fluid mixtures/suspensions, the heterogeneities are assumed to be small compared to the seismic wavelength. This step is the first step in the workflow in Fig. 1:

$$\frac{1}{K_{fluid}} = \frac{S_w}{K_{brine}} + \frac{S_g}{K_{CO_2}}, \tag{1}$$

$$\rho_{fluid} = S_w\rho_{brine} + S_g\rho_{CO_2}. \tag{2}$$

The bulk and shear moduli of mineral grains ($K_{mineral}$ and $\mu_{mineral}$) are estimated by taking Voigt-Reuss-Hill averaging[41] of the mineral constituents with published experimental moduli[8,42]. The mineral grain composition requires the mineralogy (such as quartz, clay ratio for sandstone) and literature values of bulk (K) and shear (μ) moduli to determine the density of the mineral grains ($\rho_{mineral}$) and the bulk ($K_{mineral}$) and shear ($\mu_{mineral}$) moduli of the grains. We assume 70% quartz and 30% clay. Mineral composition at a GCS site can be estimated from wireline log data acquired during site characterization[9]. We assume the bulk and shear moduli of the mineral grains ($K_{mineral}$) has little dependency on stress because of the small range of stresses within CO_2 reservoirs, while the bulk and shear moduli of the rock framework are very sensitive to stress, which we incorporate into the CO_2 rock physics model. This step is the second step in Fig. 1.

Calculation of K_{frame} with Hertz-Mindlin theory and Hashin-Strikman approaches

The first step is to determine $K_{frame} = K_{HSframe}$ using the Hertz-Mindlin model with the Hashin-Strikman lower bound. The Hertz-Mindlin model combines the normal and tangential forces of precompacted identical spheres. The Hertz-Mindlin contact theory considers the effects of pore pressure changes in Eqs. (3) and (4) in the general case. The modified Hashin-Strikman lower bound[43,44] estimates the effective bulk and shear moduli of the dry rock frame at a different porosities ϕ in Eqs. (5)–(6). The Hashin-Shtrikman bounds define a range of plausible elastic moduli for a mix of two phases, such as sand and cement/clay. The lower bound assumes the soft-sand model, which calculates moduli based on dry sand where the cement is deposited away from grain contacts. The upper bound constitutes the stiff-sand model, where cement is deposited at grain contacts. The Hertz-Mindlin theory requires elastic moduli of the mineral grains, Poisson's ratio, critical porosity, and porosity. Then, we determine K_{sat} with the Gassmann equation and the calculated K_{frame} (Eq. [(7)]).

The Hertz-Mindlin theory expression for the effective bulk and shear moduli of a dry, dense, random pack of identical spheres at the critical porosity:

$$K_{mc} = \left(\frac{C^2(1-\phi_c)^2\mu_{mineral}^2 p_d}{18\pi^2(1-\nu)^2}\right)^{1/3}, \tag{3}$$

$$\mu_{mc} = \frac{5-4\nu}{10-5\nu}\left(\frac{3C^2(1-\phi_c)^2\mu_{mineral}^2 p_d}{2\pi^2(1-\nu)^2}\right)^{1/3}. \tag{4}$$

The effective moduli at different porosities are found with the modified Hashin-Shtrikman lower bound:

$$K_{HSframe} = \left[\frac{\frac{\phi}{\phi_c}}{K_{mc}+\frac{4}{3}\mu_{mc}} + \frac{1-\frac{\phi}{\phi_c}}{K_{mineral}+\frac{4}{3}\mu_{mc}}\right]^{-1} - \frac{4}{3}\mu_{mc}, \tag{5}$$

$$\mu_{HSframe} = \left[\frac{\frac{\phi}{\phi_c}}{\mu_{mc}+\frac{\mu_{mc}}{6}\left(\frac{9K_{mc}+8\mu_{mc}}{K_{mc}+2\mu_{mc}}\right)} + \frac{1-\frac{\phi}{\phi_c}}{\mu_{mineral}+\frac{\mu_{mc}}{6}\left(\frac{9K_{mc}+8\mu_{mc}}{K_{mc}+2\mu_{mc}}\right)}\right]^{-1} - \frac{1}{6}\mu_{mc}\left(\frac{9K_{mc}+8\mu_{mc}}{K_{mc}+2\mu_{mc}}\right), \tag{6}$$

$$K_{sat} = K_{HS\,frame} + \frac{\left(1 - \frac{K_{HS\,frame}}{K_{mineral}}\right)^2}{\frac{\phi}{K_{fluid}} + \frac{1-\phi}{K_{mineral}} - \frac{K_{HS\,frame}}{K^2_{mineral}}}. \quad (7)$$

The density of the saturated rock matrix is determined using:

$$\rho_{sat} = \phi * \rho_{fluid} + (1 - \phi) * \rho_{matrix}. \quad (8)$$

Calculation of K_{frame} with Krief modeling

Another method to estimate K_{sat} is using the Krief equation that employs a different method to estimate $K_{frame} = K_{Krframe}$.

The Krief modeling only requires porosity and elastic moduli of the grains to determine the framework elastic moduli. The workflow is similar to that for updating K_{sat}, Eqs. ((9)-(12)):

$$K_{sat} = K_{Kr\,frame} + \frac{\alpha^2}{\frac{\phi}{K_{fluid}} + \frac{(\alpha-\phi)}{K_{mineral}}}, \quad (9)$$

$$\alpha = 1 - (1 - \phi)^{\frac{n}{1-\phi}}, n = 3, \quad (10)$$

$$K_{Kr\,frame} = (1 - \alpha)K_{mineral}, \quad (11)$$

$$\mu_{Kr\,frame} = (1 - \alpha)\mu_{mineral}. \quad (12)$$

Incorporating compliant porosity

The bulk and shear moduli and porosity of the dry rock frame are updated from a series of papers[21,23,24]. Any approach can be used to estimate drained rock bulk or shear moduli, such as Hashin-Strikman or Krief modeling (denoted with K_{drs}), but it must assume stiff porosity, where compliant pores are closed. We assume that $D_S = D_P = D$ in Eqs. (18) and (19). We employ a grid search for D. For each guess for D, we use a linear least-squares fit to resolve A_P, A_S, K_P, K_S, B_P, and B_S. We select the D value, which provides the minimum least-squares misfit. Each modified modulus is denoted with 'm' to consider compliant porosity with the following equations:

$$K_{drm} = K_{drys} * \left[1 + \theta_s\left(\frac{1}{K_{drys}} - \frac{1}{K_{mineral}}\right)p_d - \theta_c\phi_{c0}\exp\left(-\theta_c p_d \frac{1}{K_{drys}}\right)\right], \quad (13)$$

$$\mu_{drm} = \mu_{drys} * \left[1 + \theta_{s\mu}\left(\frac{1}{K_{drys}} - \frac{1}{K_{mineral}}\right)p_d - \theta_{c\mu}\phi_{c0}\exp\left(-\theta_c p_d \frac{1}{K_{drys}}\right)\right], \quad (14)$$

$$\phi = \phi_{s0} - \left(\frac{1}{K_{drys}} - \frac{1}{K_{mineral}}\right)p_d + \phi_{c0}\exp\left(-\theta_c p_d \frac{1}{K_{drys}}\right), \quad (15)$$

$$\phi_m(p_d) = \phi_0 + \phi_{c0}\exp\left(-\theta_c p_d \frac{1}{K_{drys}}\right). \quad (16)$$

The density of the saturated rock matrix with compliant porosity is obtained using:

$$\rho_{sat} = \phi_m * \rho_{fluid} + (1 - \phi_m) * \rho_{matrix}. \quad (17)$$

Rock measurements of V_P and V_S as a function of differential pressure can be measured and fit with a linear least-squares to the following equations. We seek the parameter, D, for the minimum misfit:

$$V_{Pdry}(p_d) = A_P + K_P p_d - B_P \exp(-p_d D), \quad (18)$$

$$V_{Sdry}(p_d) = A_S + K_S p_d - B_S \exp(-p_d D), \quad (19)$$

where,

$$\begin{array}{llll} A_P = V_{Pdrys} & & A_S = V_{Sdrys} & \\ K_P = 0.5V_{Pdrys}H_s\theta_{s\mu}\left(\frac{1}{K_{drys}} - \frac{1}{K_{mineral}}\right) & & K_S = 0.5V_{Sdrys}\theta_{s\mu}\left(\frac{1}{K_{drys}} - \frac{1}{K_{mineral}}\right) & \\ B_P = 0.5V_{Pdrys}H_c\theta_{c\mu}\phi_{c0} & & B_S = 0.5V_{Sdrys}\theta_{c\mu}\phi_{c0} & \\ D = \frac{\theta_c}{K_{drys}} & & & \\ V_{Sdrys} = \sqrt{\frac{\mu_{drys}}{\rho}} & & V_{Pdrys} = \sqrt{\frac{K_{drys}+\frac{4}{3}\mu_{drys}}{\rho}} & \end{array}$$

We use the following steps to solve for the compliant porosity parameters in Eqs. (13), (14), and (16). First, we determine the shear and bulk moduli of the dry rock matrix with close compliant pores:

$$\mu_{drys} = A_S^2\rho, \quad (20)$$

$$K_{drys} = A_P^2\rho - 4/3\mu_{drys}. \quad (21)$$

Second, we compute θ_c:

$$\theta_c = DK_{drys}. \quad (22)$$

Third, we determine $\theta_{c\mu}$:

$$\frac{B_P}{B_S} = \frac{A_P H_c}{A_S} \qquad H_c = \frac{K_{drys}\frac{\theta_c}{\theta c\mu} + 4/3\mu_{drys}}{K_{drys} + 4/3\mu_{drys}}$$

$$\theta_{c\mu} = K_{drys}\theta_c\left(\frac{B_P A_S}{B_S A_P}(K_{drys} + 4/3\mu_{drys}) - 4/3\mu_{drys}\right)^{-1}. \quad (23)$$

Then, we obtain ϕ_{c0}:

$$\phi_{c0} = \frac{2B_S}{A_S\theta_{c\mu}}. \quad (24)$$

For the stiff porosity components in Eqs. (13) and (14), we can also obtain the following:

$$\theta_{s\mu}\left(\frac{1}{K_{drys}} - \frac{1}{K_{mineral}}\right) = \frac{2K_S}{A_S} \quad (25)$$

and

$$H_s = \frac{K_{drys}\frac{\theta_s}{\theta s\mu} + 4/3\mu_{drys}}{K_{drys} + 4/3\mu_{drys}}$$

$$\theta_s\left(\frac{1}{K_{drys}} - \frac{1}{K_{mineral}}\right) = K_{drys}^{-1} * \left[2K_P A_P\rho - 8/3\mu_{drys}K_S * A_S^{-1}\right]. \quad (26)$$

Data availability

The study has not generated new raw data. The datasets utilized in the analysis are publicly available, with appropriate links for each one found in the reference list, but we have included data we used in creating figures for this study. Data used to generate the figures in this paper is available in. csv

format at https://doi.org/10.5281/zenodo.11477697. The Kimberlina-1.2 dataset can be found in EDX.

Code availability

The code associated with this paper is available pending on LANL's approval for release.

Received: 3 April 2023; Accepted: 5 June 2024;
Published online: 17 June 2024

References

1. Daley, T., Harbert, W., Davis, T., Landrø, M. & Wilson, M. Goals of CO_2 monitoring: why and how to access the subsurface changes associated with ccs. *Geophys. Geosequestration*, **1**, 54–70 (2019).
2. Chadwick, R. et al. 4d seismic imaging of an injected CO2 plume at the sleipner field, central north sea. *Geol. Soc. Lond. Mem.* **29**, 311–320 (2004).
3. Meadows, M. A. & Cole, S. P. 4d seismic modeling and CO2 pressure-saturation inversion at the weyburn field, saskatchewan. *Int. J. Greenh. Gas. Control* **16**, S103–S117 (2013).
4. Souza, R. & Lumley, D. Estimation of reservoir fluid saturation from seismic data: amplitude analysis and impedance inversion as a function of noise. *ASEG Ext. Abstr.* **2015**, 1–4 (2015).
5. Huang, L. & Yang, X. Geophysical monitoring techniques: Current status and future directions. In *Geophysical Monitoring for Geologic Carbon Storage,* L. Huang (Ed.), 439–440 (AGU-Wiley, 2022).
6. Gassmann, F. Uber die elastizitat poroser medien. *Vierteljahrsschr. der Naturforschenden Ges. Zur.* **96**, 1–23 (1951).
7. Biot, M. A. General theory of three-dimensional consolidation. *J. Appl. Phys.* **12**, 155–164 (1941).
8. Roach, L. A., White, D. J. & Roberts, B. Assessment of 4d seismic repeatability and CO2 detection limits using a sparse permanent land array at the aquistore CO_2 storage site. *Geophysics* **80**, WA1–WA13 (2015).
9. Wang, Z., Harbert, W. P., Dilmore, R. M. & Huang, L. Modeling of time-lapse seismic monitoring using CO2 leakage simulations for a model CO_2 storage site with realistic geology: application in assessment of early leak-detection capabilities. *Int. J. Greenh. Gas. Control* **76**, 39–52 (2018).
10. Harbert, W. & Lipinski, B. Technologies monitor CO_2 EOR floods. *American Oil and Gas Reporter* 119–123 (2010).
11. Lei, X. & Xue, Z. Ultrasonic velocity and attenuation during co2 injection into water-saturated porous sandstone: measurements using difference seismic tomography. *Phys. Earth Planet. Inter.* **176**, 224–234 (2009).
12. Shi, J.-Q., Xue, Z. & Durucan, S. Seismic monitoring and modelling of supercritical CO_2 injection into a water-saturated sandstone: Interpretation of p-wave velocity data. *Int. J. Greenh. Gas. Control* **1**, 473–480 (2007).
13. Xue, Z. & Ohsumi, T. Seismic wave monitoring of CO_2 migration in water-saturated porous sandstone. *Exploration Geophys.* **35**, 25–32 (2004).
14. Harbert, W. et al. CO_2 induced changes in mount simon sandstone: understanding links to post CO_2 injection monitoring, seismicity, and reservoir integrity. *Int. J. Greenh. Gas. Control* **100**, 103109 (2020).
15. Sun, L., Jessen, K. & Tsotsis, T. T. Impact of exposure to brine/CO_2 on the mechanical and transport properties of the mt. simon sandstone. *Greenh. Gases: Sci. Technol.* **11**, 1043–1055 (2021).
16. Vafaie, A., Cama, J., Soler, J. M., Kivi, I. R. & Vilarrasa, V. Chemo-hydro-mechanical effects of co2 injection on reservoir and seal rocks: A review on laboratory experiments. *Renew. Sustain. Energy Rev.* **178**, 113270 (2023).
17. Al-Hosni, M., Vialle, S., Gurevich, B. & Daley, T. Effect of CO2 on rock properties: Frio crosswell case study. In *Third EAGE Workshop on Rock Physics*, vol. 2015, 1–6 (European Association of Geoscientists & Engineers, 2015).
18. Al Hosni, M., Vialle, S., Gurevich, B. & Daley, T. M. Estimation of rock frame weakening using time-lapse crosswell: The frio brine pilot project. *Geophysics* **81**, B235–B245 (2016).
19. Ivandic, M. et al. Geophysical monitoring at the ketzin pilot site for CO2 storage: New insights into the plume evolution. *Int. J. Greenh. Gas. Control* **32**, 90–105 (2015).
20. Johnson, P. & Rasolofosaon, P. Manifestation of nonlinear elasticity in rock: convincing evidence over large frequency and strain intervals from laboratory studies. *Nonlinear Process. Geophys.* **3**, 77–88 (1996).
21. Shapiro, S. A. & Kaselow, A. On the stress dependence of seismic velocies in porous rocks. In *2002 SEG Annual Meeting* (OnePetro, 2002).
22. Shapiro, S. A. Elastic piezosensitivity of porous and fractured rocks. *Geophysics* **68**, 482–486 (2003).
23. Shapiro, S. A. & Kaselow, A. Porosity and elastic anisotropy of rocks under tectonic stress and pore-pressure changes. *Geophysics* **70**, N27–N38 (2005).
24. Shapiro, S. et al. Permeability dependency on stiff and compliant porosities: a model and some experimental examples. *J. Geophys. Eng.* **12**, 376–385 (2015).
25. Prasad, M., Glubokovskikh, S., Daley, T., Oduwole, S. & Harbert, W. CO_2 messes with rock physics. *Lead. Edge* **40**, 424–432 (2021).
26. Gasperikova, E. et al. Kimberlina 1.2 ccus geophysical models and synthetic data sets. Tech. Rep., National Energy Technology Laboratory (NETL), Pittsburgh, PA, Morgantown, WV (2022) https://edx.netl.doe.gov/dataset/kimberlina-1-2-ccus-geophysical-models-and-synthetic-data-sets.
27. Alumbaugh, D. et al. The kimberlina synthetic multiphysics dataset for co2 monitoring investigations. *Geosci. Data J.* **11**, 216–234 (2023).
28. Bell, I. H., Wronski, J., Quoilin, S. & Lemort, V. Pure and pseudo-pure fluid thermophysical property evaluation and the open-source thermophysical property library coolprop. *Ind. Eng. Chem. Res.* **53**, 2498–2508 (2014).
29. Batzle, M. & Wang, Z. Seismic properties of pore fluids. *Geophysics* **57**, 1396–1408 (1992).
30. Mindlin, R. D. Compliance of elastic bodies in contact. *J. Appl. Mech.* **16**, 259–268 (1949).
31. Krief, M., Garat, J., Stellingwerff, J. & Ventre, J. A petrophysical interpretation using the velocities of p and s waves (full-waveform sonic). *The Log Analyst* **31**, 355–367 (1990).
32. Geertsma, J. The effect of fluid pressure decline on volumetric changes of porous rocks. *Trans. AIME* **210**, 331–340 (1957).
33. Skempton, A. Horizontal stresses in an overconsolidated eocene clay. *SELECTED PAPERS ON SOIL MECHANICS* **1**, 119–125 (1961).
34. Zimmerman, R. W., Somerton, W. H. & King, M. S. Compressibility of porous rocks. *J. Geophys. Res.: Solid Earth* **91**, 12765–12777 (1986).
35. Delaney, D. et al. Dynamic moduli and attenuation: Rhyolite and carbonate examples. In *Geophysical Monitoring for Geologic Carbon Storage* L. Huang (Ed.), 73–92 (AGU-Wiley, 2022).
36. Fuchs, S. J., Espinoza, D. N., Lopano, C. L., Akono, A.-T. & Werth, C. J. Geochemical and geomechanical alteration of siliciclastic reservoir rock by supercritical CO2-saturated brine formed during geological carbon sequestration. *Int. J. Greenh. Gas. Control* **88**, 251–260 (2019).
37. Akono, A.-T. et al. A review of geochemical–mechanical impacts in geological carbon storage reservoirs. *Greenh. Gases: Sci. Technol.* **9**, 474–504 (2019).
38. Gasperikova, E. et al. Sensitivity of geophysical techniques for monitoring secondary co2 storage plumes. *Int. J. Greenh. Gas. Control* **114**, 103585 (2022).
39. Wood, A. B. & Lindsay, R. A textbook of sound. *Phys. Today* **9**, 37 (1956).
40. Kumar, M. K., Sateesh, B., Prabhakar, S., Sastry, G. N. & Vairamani, M. Generation of regiospecific carbanions under electrospray ionisation conditions and their selectivity in ion-molecule reactions with CO2.

Rapid Commun. Mass Spectrom.: Int. J. Devoted Rapid Dissem. Minute Res. Mass Spectrom. **20**, 987–993 (2006).
41. Hill, R. The elastic behaviour of a crystalline aggregate. *Proc. Phys. Soc. Sect. A* **65**, 349 (1952).
42. Kimizuka, H., Ogata, S. & Shibutani, Y. Atomistic characterization of structural and elastic properties of auxetic crystalline sio2. *Phys. Status Solidi B* **244**, 900–909 (2007).
43. Dvorkin, J. & Nur, A. Elasticity of high-porosity sandstones: Theory for two north sea data sets. *Geophysics* **61**, 1363–1370 (1996).
44. Hashin, Z. & Shtrikman, S. A variational approach to the theory of the elastic behaviour of multiphase materials. *J. Mech. Phys. Solids* **11**, 127–140 (1963).
45. Purcell, C. et al. Velocity measurements in reservoir rock samples from the sacroc unit using various pore fluids, and integration into a seismic survey taken before and after a CO2 sequestration flood. *Energy Procedia* **1**, 2323–2331 (2009).

Acknowledgements

This work was completed as part of the National Risk Assessment Partnership (NRAP) project with support from the U.S. Department of Energy (DOE) Office of Fossil Energy's Crosscutting Research Program through the Los Alamos National Laboratory (LANL) operated by Triad National Security LLC for the U.S. DOE National Nuclear Security Administration (NNSA) under Contract No. 89233218CNA000001, and through Lawrence Berkeley National Laboratory under Contract No. DE-AC02-05CH1123. LANL approved for public release under LA-UR 23-22625. We thank the generous contributions of two anonymous reviewers.

Author contributions

N.C., L.H., and W.H. conceived the project. N.C. performed the work and analyzed the results. L.H. initiated the research idea and obtained funding. W.H. provided laboratory data. T.B. suggested the Krief modeling. E.G and Q.Z. provided Kimberlina-1.2 reservoir modeling outputs. All authors contributed feedback to this work and reviewed the manuscript.

Competing interests

The authors declare no competing interests.

Additional information

Supplementary information The online version contains supplementary material available at https://doi.org/10.1038/s43247-024-01493-6.

Correspondence and requests for materials should be addressed to Neala Creasy or Lianjie Huang.

Peer review information *Communications Earth & Environment* thanks Serge Shapiro and the other, anonymous, reviewer(s) for their contribution to the peer review of this work. Primary Handling Editors: Luca Dal Zilio and Joe Aslin. A peer review file is available.